A Comparative Study of Two Permanent Magnet Motors Structures with Interior and Exterior Rotor

Mohamed Chaieb [1], Naourez Ben Hadj [2], Jalila Kaouthar Kammoun [3], and Rafik Neji [4]

[1] *Electrical Engineering Department, University of Sfax, chaieb_med@yahoo.fr*
[2] *Electrical Engineering Department, University of Sfax, benhadj.naourez@enis.rnu.tn*
[3] *Electrical Engineering Department, University of Sfax, kaoutharkammoun@yahoo.fr*
[4] *Electrical Engineering Department, University of Sfax, rafik.neji@enis.rnu.tn*

Abstract
Currently, the permanent magnet motors PMM represent an attractive solution in the electric traction field, thanks to their higher performances than other electric motors. In this context, this work represents an analytical study and validation by the finite element method of two configurations, the radial flux permanent magnet synchronous motors with exterior rotor PMSMER and with interior rotor PMSMIR. This paper is divided into two sections: In the first section, we represent the analytical study based on electromagnetic law of the two structures PMSMER and PMSMIR. In the second section, we represent a comparative study of the two structure performances.

Keywords
permanent magnet motors design, radial flux, finite element method, modelling, performance

1. INTRODUCTION
Considering the large variety of electric motors, such as asynchronous motors, synchronous motors with variable reluctances, permanent magnet motors with radial or axial flux, the committed firms try to find the best choice of the motor conceived for electric vehicle field.
There are different criteria of selection in order to solve this problem such as the power-to-weight ratio, the efficiency and the price. The traction electric motor is specified by several qualities, such as the flexibility, reliability, cleanliness, facility of maintenance, silence etc. Moreover, it must satisfy several requirements, for example the possession of a high torque and an important efficiency [Zire et al., 2003; Gasc, 2004; Chan, 2004].
In this context, The PMM is characterized by a high efficiency, very important torque, and power-to-weight, so it becomes very interesting for electric traction. The rotor of the PMM supports several configurations interesting for the magnets mounted on surface.
In the intension, to ensure the most suitable and judicious choice, we start by a comparative study between the two structures, then, we implement a methodology of design based on an analytical modelling and on the electromagnetism laws.

2. MODELLING OF THE TWO PMM STRUCTURES
2.1 Structural data
The motors structure allowing the determination of the studied geometry is based on three relationships.
The ratio β is the relationship between the magnet angular width L_a and the pole-pitch L_p. This relationship is used to adjust the magnet angular width according to the motor pole-pitch.

$$\beta = \frac{L_a}{L_p} \tag{1}$$

$$L_p = \frac{\pi}{P} \tag{2}$$

The ratio R_{ldla} is the relationship between the angular width of a principal tooth and of the magnet angular width. This ratio is responsible for the regulation of the principal tooth size which has a strong influence on the electromotive force form.

$$R_{ldla} = \frac{A_{dent}}{L_a} \tag{3}$$

The R_{did} ratio is the relationship between the principal tooth angular width and the inserted tooth angular width A_{denti}. This relationship fixes the inserted tooth size.

$$R_{did} = \frac{A_{dent}}{L_a} \tag{4}$$

2.2 Geometrical structures of the PMSMIR and the PMSMER

This part is devoted to an analytical sizing allowing calculation of geometrical sizes of the two PMM configurations which are the PMSMER and the PMSMIR. Figure 1 represents the PMSMER and the PMSMIR with the number of pole pairs is 4 and a number of principal teeth is 6, between two principal teeth, an inserted tooth is added to improve the form of wave and to reduce the leakage flux [Hadj et al., 2007]. The slots are right and open in order to facilitate the insertion of coils and to reduce the production cost. The type of winding is concentric; each winding of phase is made up of two diametrically opposite coils [Magnussen et al., 2005; Bianchi et al., 2003; Libert and Soulard, 2004].

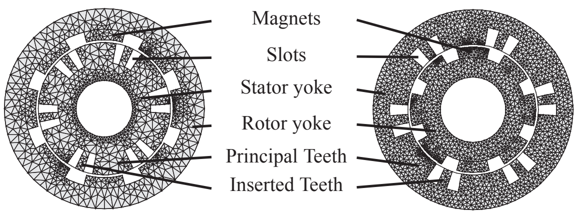

Fig. 1 Radial flux permanent magnet motors with exterior rotor and interior rotor

2.3 Analytical sizing of the two motors structures

The analytical study of motor sizing is based on the schedules conditions parameters, the constant characterizing materials, the expert data and the configuration of the two motors. This Sizing motor approach is represented as follows:

2.3.1 The schedules data conditions

- Electric vehicle mass M = 1000 kg
- Angle of starting $a_d = 3$ °
- Time of starting $t_d = 4$ s
- Outside temperature $t_{ex} = 40$ °C
- Maximum motor power $P_{mmax} = 21{,}635$ kW
- Winding temperature $t_b = 95$ °C
- Base speed of the vehicle $V_b = 30$ km/h
- Maximum Speed of the vehicle $V_{max} = 100$ km/h
- Load factor of the slots $k_r = 0, 44$
- Acceptable density of current in the slots $\delta = 7$ A/mm^2

2.3.2 Constants specific to materials

The motor is composed by a diversity of materials specified as follows:

- Remanent magnetic induction of the magnets $B_m = 1{,}175$ T
- Induction of demagnetization $B_c = 0{,}383$ T
- Magnetic induction in teeth data base = 0,9 T
- Relative permeability of the magnets $\mu_a = 1{,}05$ H/m
- Coefficient of mechanical losses $k_m = 1$ %
- Resistivity of copper with 95 °C $R_{cu} = 17{,}2\ 10^{-9}$ Ωm
- Coefficient of variation of the copper resistivity α = 0,004
- Density of the electrical sheets $M_{vt} = 7850$ kg
- Density of magnets $M_{va} = 7400$ kg
- Density of copper $M_{vc} = 8950$ kg
- Coefficient of quality of the sheets Q = 1,100
- Density of copper $M_{vc} = 8950$ kg

2.3.3 Expert data

The expert data are practically represented by three sizes which are, the magnetic induction in the air gap Be, the magnetic induction in the stator yoke Bcs and the magnetic induction in the rotor yoke B_{cr}. It should be noted that the zone of variation of these three parameters varies between 0,2 to 1,6 T [Hadj et al., 2007].

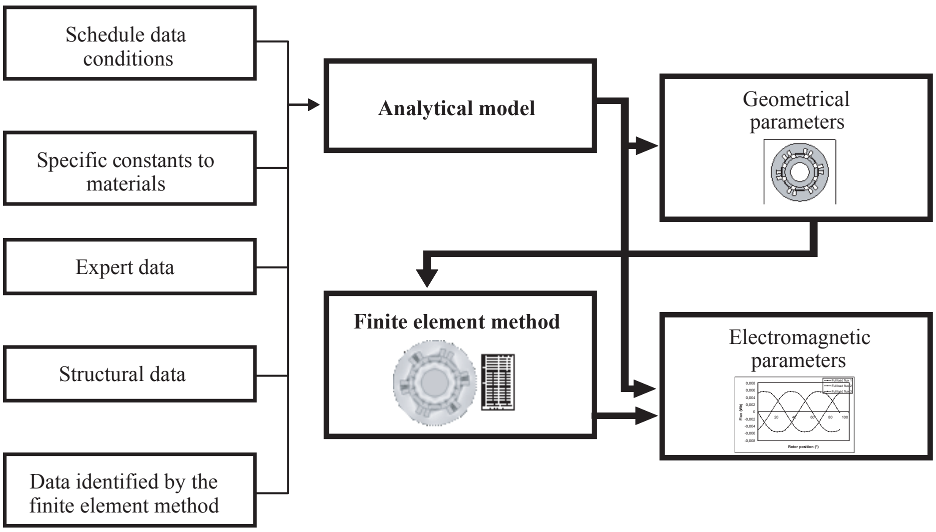

Fig. 2 Sizing motor approach

2.3.4 Structural data

For the two configurations, we adopted the same number of pole pairs P = 4, with an air gap thickness equivalent to 2mm, With a relationship β equal to 0,667 and R_{ldla} equal to 1,2.

2.3.5 Data identified by the finite element method

K_{fu} is the flux leakage coefficient of the PMSMIR which is fixed to 0,95 whereas for the PMSMER, K_{fu} is equal to 0,98. Between the principal tooth angular width A_{dent} and the inserted tooth angular width A_{denti}, we define a ratio R_{did} equal to 0,2.

2.4 Geometrical sizes

Geometrical parameters of the two structures motors are defined in Figure 3.

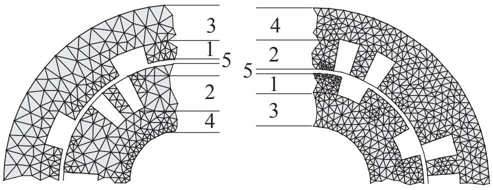

1 : The magnet height, h_a
2 : The slots height and the tooth height, h_e, h_d
3 : The rotor yoke height, h_{cr}
4 : The stator yoke height, h_{cs}
5 : The air gap thickness, e

Fig. 3 PMSMER and PMSMIR parameters

2.4.1 Stator geometrical sizes of the PMSMIR

The slot average width: L_{enc}

$$L_{enc} = \frac{D_m + e + H_d}{2} A_{enc} \tag{5}$$

The principal tooth section: S_d

$$S_d = \frac{D_m + e}{2} A_{dent} L_m \tag{6}$$

The inserted tooth section: S_{di}

$$S_{di} = \frac{D_m + e}{2} A_{denti} L_m \tag{7}$$

The slot section: S_e

$$S_e = A_{enc}\frac{D_m + e}{2} L_m = \frac{1}{2}\left[\frac{2\pi}{Nd} - A_{dent} - A_{denti}\right]\frac{D_m + e}{2} L_m \tag{8}$$

2.4.2 Stator geometrical sizes of the PMSMER

The slot average width: L_{enc}

$$L_{enc} = \frac{D_m - e - H_d}{2} A_{enc} \tag{9}$$

The principal tooth section: S_d

$$S_d = \frac{D_m - e}{2} A_{enc} L_m \tag{10}$$

The inserted tooth section: S_{di}

$$S_{di} = \frac{D_m + e}{2} A_{denti} L_m \tag{11}$$

The slot section: S_e

$$S_e = A_{enc}\frac{D_m - e}{2} L_m = \frac{1}{2}\left[\frac{2\pi}{N_d} - A_{dent} - A_{denti}\right]\frac{D_m - e}{2} L_m \tag{12}$$

with L_m is the motor length.

The teeth height H_d of the PMSMIR is expressed by equation 13 with N_{sph} is the number of turns per phase and In is the rated current.

H_d specific to the PMSMIR is expressed:

$$H_d = \sqrt{\frac{N_{sph}.I_n}{N_d \delta K_r A_{enc}} + \left(\frac{D_m + e}{2}\right)^2} - \frac{D_m + e}{2} \tag{13}$$

H_d specific to the PMSMER is expressed:

$$H_d = \sqrt{\frac{N_{sph}.I_n}{N_d \delta K_r A_{enc}} + \left(\frac{D_m - e}{2}\right)^2} - \frac{D_m - e}{2} \tag{14}$$

The stator yoke thickness H_{cs} is obtained by application of the flux conservation theorem.

$$H_{cs} = \frac{B_d S_d}{2 L_m B_{cs}} \tag{15}$$

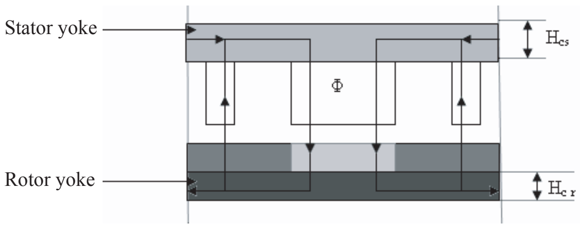

Fig. 4 Application of the theorem of the flux conservation

2.4.3 The rotor geometrical sizes of the two structures

The expression of the magnet height H_a is the same one in the two structures; it is obtained by the application of the Ampere theorem:

$$\int_{contour} \vec{H} d\vec{l} = \Sigma ni \Leftrightarrow H_a h_a + e h_e = 0 \tag{16}$$

The remanent induction of the magnet $M_{(Ta)}$ at T_a °C is defined by:

$$H_a = \frac{\mu_a B_e e}{M_{(Ta)} - \dfrac{B_e}{K_{fu}}} \tag{17}$$

$$M_{(Ta)} = M\left[1 + \alpha_m (T_a - 20)\right] \tag{18}$$

The rotor yoke thickness H_{cr} is defined:

$$\frac{\Phi}{2} = B_{cs} H_{cr} L_m K_{fu} = \frac{B_e S_d}{2} \Leftrightarrow H_{cr} = \frac{B_e S_d}{2 K_{fu} L_m B_{cr}} \tag{19}$$

2.4.4 Electrical sizing

The electromotive force in the two structures is expressed by:

$$EMF_1(t) = \frac{8}{\pi} N_{sph} L_m D_m B_e \sin\left(\frac{\pi}{2}\beta\right) \sin\left(\frac{\pi}{2}\beta R_{ldla}\right) \Omega_m \sin\left(P\Omega_m t\right) \tag{20}$$

The motor electric constant: K_e

$$K_e = \frac{12}{\pi} N_{sph} L_m D_m B_e \sin\left(\frac{\pi}{2}\beta\right) \sin\left(\frac{\pi}{2}\beta R_{ldla}\right) \tag{21}$$

The electromagnetic torque: T_{em}

$$T_{em}(t) = \frac{1}{\Omega} \sum_{i=1}^{3} EMF_i(t).i_i(t) \tag{22}$$

with EMFi and i_i respectively represent the electromotive force and the current of the i phase.

The motor rated current I_n is the ratio between the electromagnetic torque and the motor electric constant

$$I_n = \frac{T_{em}}{K_e} \tag{23}$$

The phase résistance of the motor: R_{ph}

$$R_{ph} = R_{cu}(Tb) \frac{N_{sph} \delta L_{sp}}{I_n / \sqrt{2}} \tag{24}$$

where $R_{cu}(Tb)$ is the Resistivity of copper at the temperature of winding T_b and L_{sp} is the spire average length defined as follow [Hadj et al., 2007].

$$R_{cu}(Tb) = R_{cu}\left[1 + \alpha (Tb - 20)\right] \tag{25}$$

$$L_{sp} = 2\left((A_{enc} + A_{dent}).\left(\frac{D_m + e + h_d}{2}\right) + L_m \right) \tag{26}$$

3. COMPARATIVE STUDY BETWEEN THE TWO STRUCTURES

In this study, the validation and comparation between the two structures is based on the finite elements method using the software FEMM. The mesh in the

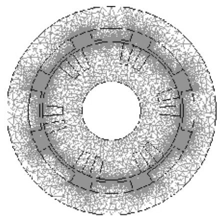

Fig. 5 Mesh in the PMSMIR

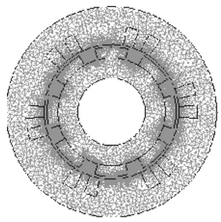

Fig. 6 Mesh in the PMSMER

two studied structures is given by figures 5 and 6, we make a refined mesh in the air gap to obtain a precised result [Ohyama et al., 2005].

Figure 7 and figure 8 show respectively the flux density in the PMSMER and in the PMSMIR.

We note that the maximal induction for the motor yokes is equal to 1.4 T that proves no saturation in magnetic motor circuit.

We note the appearance of leakages flux in the motor, this requires the determination of the leakages flux co-

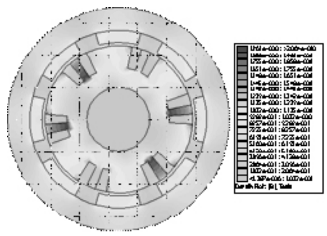

Fig. 7 Flux density in the PMSMER

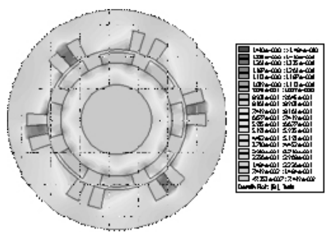

Fig. 8 Flux density in the PMSMIR

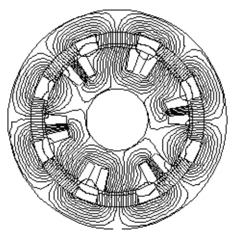

Fig. 9 Flux lines in the PMSMER

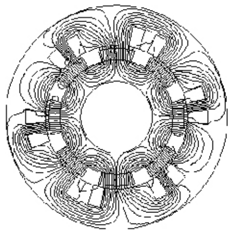

Fig. 10 Flux lines in the PMSMIR

efficient to validate the analytical model.

3.1 Electromagnetic parameters

3.1.1 Air gap flux density

Figures 11 and 12 show the airgap induction in the PMSMER and in the PMSMIR, the maximal value is about 1 T [Pakdel, 2009].

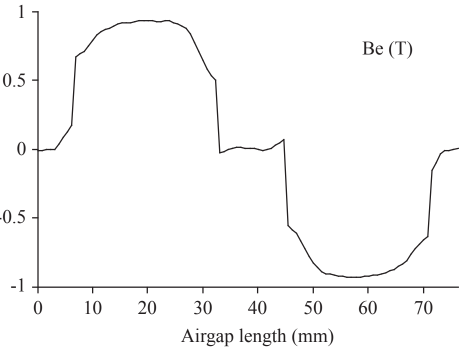

Fig. 11 Airgap induction in the PMSMER

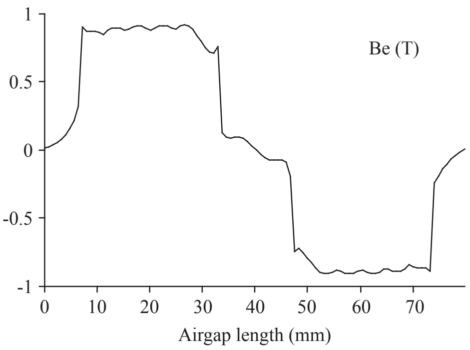

Fig. 12 Airgap induction in the PMSMIR

3.1.2 Flux

Figures 13, 14, 15 and 16 illustrate the three phases flux at no-load and at full load according to the mechanical angle for the PMSMIR and PMSMER.

According to the Figure 17, we can conclude that the variation of the flux at no-load and at full-load according to the rotor position is very weak, that originates the magnetic reaction.

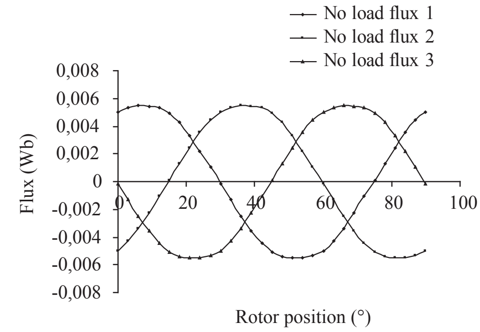

Fig. 13 Flux of the three phases at no-load for the PMSMIR

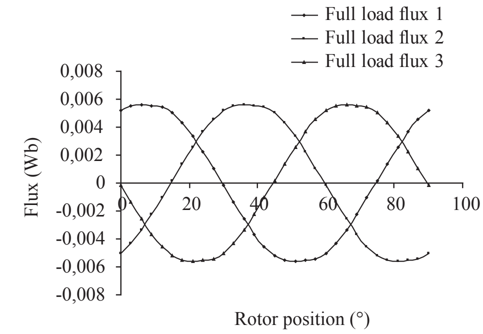

Fig. 14 Flux of the three phases at full-load for the PMSMIR

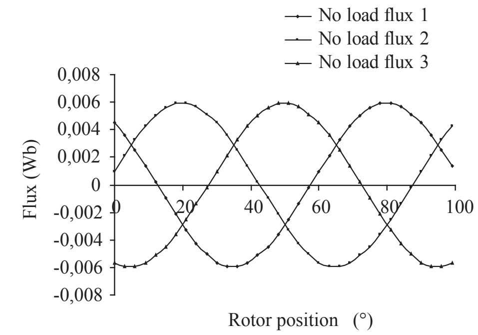

Fig. 15 Flux of the three phases at no-load for the PMSMER

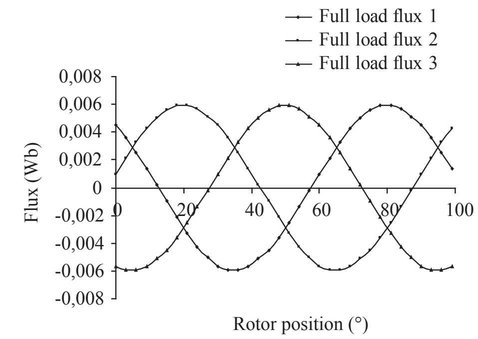

Fig. 16 Flux of the three phases at full-load for the PMSMER

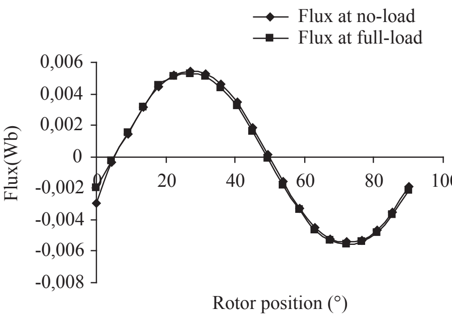

Fig. 17 Flux at Full-load and at no-load of the PMSMIR

3.1.3 Electromotive forces EMF

The form of EMF represents a very significant parameter. It is expressed by:

$$\mathrm{EMF} = -N_{sph}\frac{d\Phi}{dt} \tag{27}$$

Figures 18, 19, 20 and 21 give an idea on the form of the EMF at no-load and at full load according to the rotor position. This EMF is generated by the flux evolution through a coil of the stator.

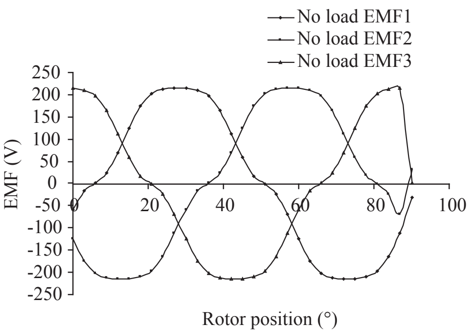

Fig. 18 EMF at no-load of the PMSMIR

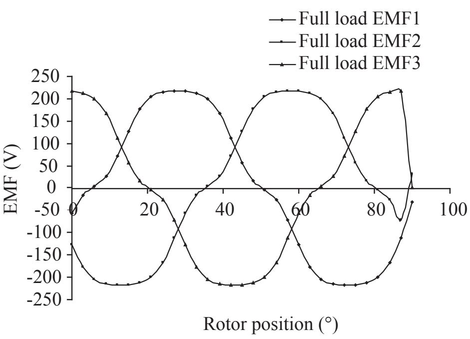

Fig. 19 EMF at full-load of the PMSMIR

3.2 Torque and Power-to-weight ratio

3.2.1 Calculation of the torque

The instantaneous torque is expressed by equation 22. Figure 22 and 23 represent the torque at full-load

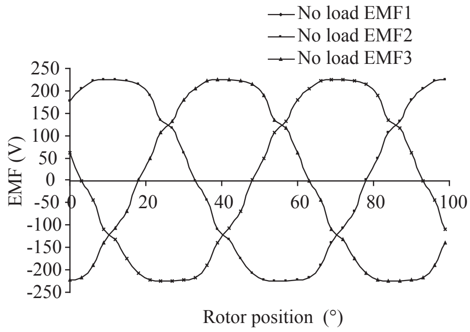

Fig. 20 EMF at no-load of the PMSMER

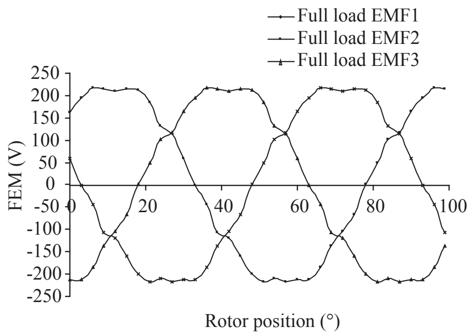

Fig. 21 EMF at full-load of the PMSMER

and at no load of the two structures obtained by the finite element method [Zhu et al., 2006; Yee-pien et al., 2009]. The obtained results validate the analytical model because the torque oscillates around the average value found analytically which is 112 Nm.

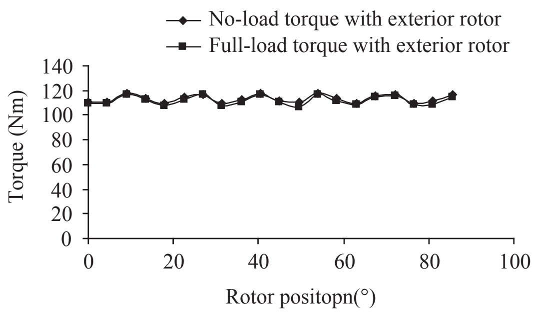

Fig. 22 Torque at no-load and at full-load for the PMSMER

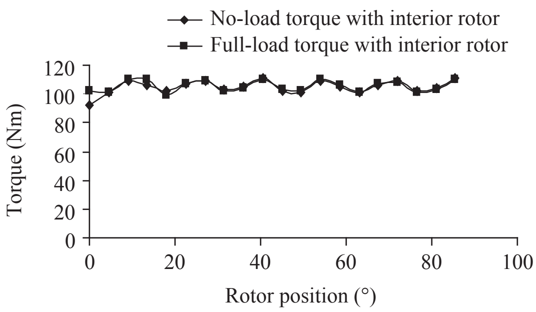

Fig. 23 Torque at no-load and at full-load for the PMSMIR

Figures 24 and 25 illustrate the torque ripple in the two structures, we conclude that the torque ripple in the PMSMER is 6.14 % and in the PMSMIR is 9.43 % [Wang et al., 2009].

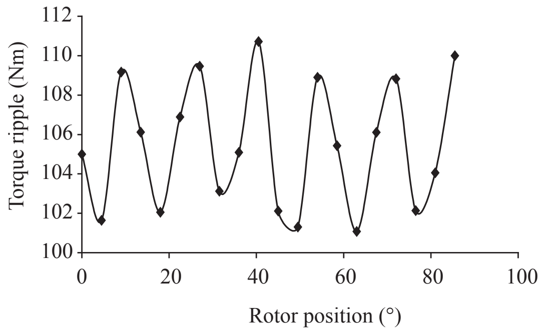

Fig. 24 Torque ripple in the PMSMER

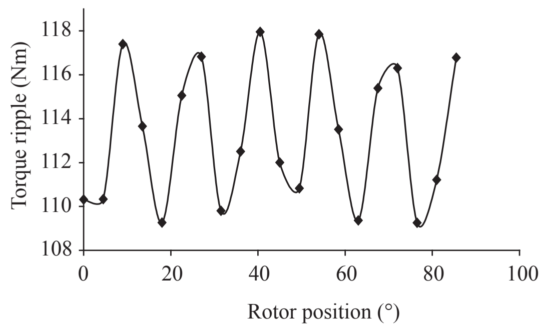

Fig. 25 Torque ripple in the PMSMIR

3.2.2 Power-to-weight ratio

The power-to-weight ratio is defined by the relationship between the power and the mass of the motor active part. Figure 26 represents the power-to-weight ratio specific to the two structures according to the power.

According to this figure, we notice that the power-to-weight ratio of the PMSMER is slightly lower than the PMSMIR, while the great motor power it is the reverse.

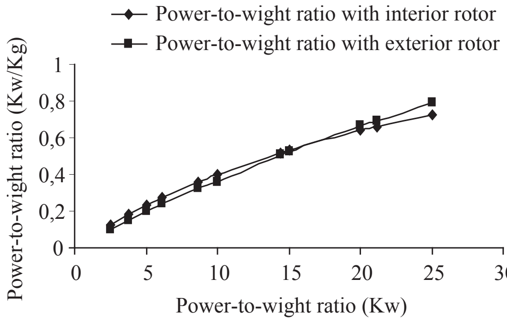

Fig. 26 Power-to-weight ratio

3.3 Losses and efficiency

Table 1 represents the efficiency and the losses for the PMSMIR and the PMSMER.

Table 1 Losses and the efficiency of the two structures

	PMSMIR	PMSMER
Joule losses	557,180	547,089
Iron losses	59,662	32,653
Mechanical losses	215,755	216,025
Efficiency	0,962	0,964

We can deduce that the Joules losses and the iron losses for the PMSMER are lower than those of the PMSMIR. Moreover, the efficiency of the PMSMER is more interesting than the other structure. Figure 27 illustrates the total losses of the two structures.

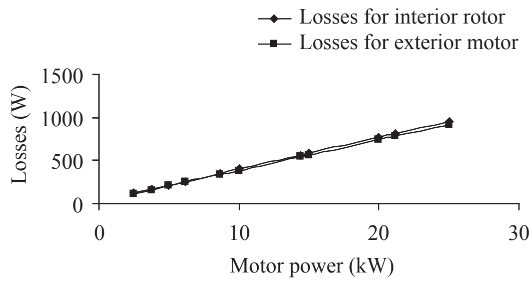

Fig. 27 Losses according to the power

We conclude that the losses magnitude is the same orders for low powers in the two structures.

However, for the powers higher than 15kW, the losses in PMSMER are lower than those produced by the PMSMIR.

Figure 28 represents the efficiency obtained for the two structures; we note that the PMSMER offers efficiency better than that developed by the PMSMIR.

As a conclusion, the configuration of the PMSMER is most suitable since it offers efficiency higher than that

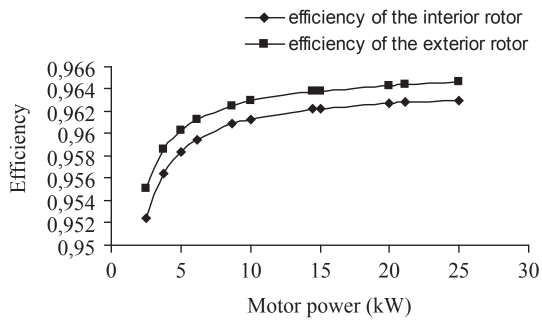

Fig. 28 Efficiency according to the power

reached by the first structure. This type of configuration is adapted more to be exploited as a motor-wheel.

4. CONCLUSION

We choose the synchronous permanent magnet motor with radial flux. Basing on the schedule data conditions, sizing approach given by Figure 2, electromagnetic laws, an analytical modelling of two structures which are the PMSMER and the PMSMIR is carried out.

We compare efficiency, mass, torques and losses in the two structures of the PMM. In conclusion, the PMSMER is the most interesting since it is more profitable and lighter than the PMSMIR. Finally, the realization of a prototype is necessary to confirm our study.

References

Bianchi, B., N. Bolognani, and P. Frare, Design Criteria for High-efficiency SPM Synchronous Motors, *IEEE Transactionss on Magnet*, Vol. 21, No. 2, 396-404, 2006.

Chan, C. C., The sate of the art of electric vehicles, *Journal of Asian Electric Vehicles*, Vol. 2, No. 2, 579-600, 2004.

Gasc, L., Permanent magnet motor design with low torque ripple for automotive electric power steering: Structure and control approaches, *PhD Thesis, Polytechnic National Institute of Toulouse*, 2004.

Hadj, N. B., S. Tounsi, R. Neji, and F. Sellami, Real coded Genetic algorithm for permanent magnet motor mass minimization for electric vehicle application, *Proceedings of 3rd International Symposium on Computational Intelligence and Intelligent Informatics*, 153-158, 2007.

Kazuhiro, O., A. Kenichi, N. Maged, F. Nashed, H. Fujii, and H. Uehara, Design using finite element analysis of switched reluctance motor for electric vehicle, *Journal of Asian Electric Vehicles*, Vol. 3, No. 2, 793-800, 2005.

Libert, F., and J. Soulard, Investigation on pole-slot combinations for permanent magnet machines with concentrated windings, *Proceedings of the International Conference on Electrical Machines*, Vol. 1, 530-535, 2004.

Magnussen, F., and H. Lendenmann, Parasitic effects in PM machines with concentrated windings, *IAS2005 40th Annual Meeting Hong Kong*, Vol. 2, 1045-1049, 2005.

Pakdel, M., Analysis of the magnetic flux density, the magnetic force and the torque in a 3D brushless DC motor, *Journal of Electromagnetic Analysis and Applications*, Vo. 1, No. 1-5, 2009.

Wang, Y., J. Shen, Z. Fang, and W. Fei, Reduction of cogging torque in permanent magnet flux-switching machines, *Journal of Electromagnetic Analysis and Applications*, Vol. 1, No. 1, 11-14, 2009.

Yee-pien, Y., Y. Shih-chin, and L. Jieng-jang, Optimal design and control of a torque motor for machine tools, *Journal of Electromagnetic Analysis and Applications*, Vol. 1, No. 4, 220-228, 2009.

Zhu, Z. Q., Y. F. Shi, and D. Howe, Comparison of torque-speed characteristics of interior-magnet machines in brushless AC and DC modes for EV/HEV applications, *Journal of Asian Electric Vehicles*, Vol. 4, No. 1, 843-850, 2006.

Zire, H. S., C. Espanet, and A. Miraoui, Performance comparison of two magnet synchronous motors structures with interior rotor and exterior rotor, *Proceedings of Electrotechnique du Futur*, EF, 51, 2003.

(Received February 5, 2010; accepted May 3, 2010)